

Diamond-shaped evolution of the superconducting interference pattern in NbTiN weak-link Josephson junctions

Kui Zhao,^{1,2,*} Huaiyuan Liu,^{1,2,*} Jianfei Xiao,^{1,2,*} Linfeng Tu,^{1,3} Jiangbo He,¹ Mingli Liu,^{1,2} Ruiyang Jiang,^{1,2} Zhongmou Jia,^{1,2} Shang Zhu,^{1,2} Yunteng Shi,^{1,2} Yiwen Ma,^{1,2} Zhaozheng Lyu,¹ Jie Shen,^{1,4} Guangtong Liu,^{1,4} Li Lu,^{1,2,4,†} and Fanming Qu^{1,2,4,‡}

¹*Beijing National Laboratory for Condensed Matter Physics,
Institute of Physics, Chinese Academy of Sciences, Beijing 100190, China.*

²*School of Physical Sciences, University of Chinese Academy of Sciences, Beijing 100049, China.*

³*School of Physics, Nankai University, Tianjin 300071, China.*

⁴*Songshan Lake Materials Laboratory, Dongguan, Guangdong 523808, China.*

(Dated: March 13, 2023)

Introducing an in-plane magnetic field into Josephson junctions is of fundamental significance in exploring a variety of interesting physical phenomena. However, extra care must be paid in realistic experiments involving an in-plane magnetic field, because trivial orbital effect due to, e.g., rippled structures can inevitably be introduced, which could produce false effect confusing the expected physical phenomena. In this work, we report a diamond-shaped evolution of the critical supercurrent in an in-plane magnetic field in NbTiN weak-link Josephson junctions. Upon application of an in-plane magnetic field perpendicular to the current, the superconducting interference pattern exhibits a characteristic evolution, which manifests as a diamond block diagram featured with each node opened and stretched out in a V-shape, mimicking the suppression-recovery patterns of critical supercurrent related to the Zeeman-driven $0 - \pi$ transition. However, the effect of Zeeman splitting plays a negligible role due to the relatively small magnetic field involved in our experiment. Therefore, we explore the trivial orbital effect of rippled structures and further take into account non-uniform current distributions pertaining in our junctions. We find that the ripples in combination with specific current distributions can give rise to a similar evolution pattern as the experimental observations. Our results serve as a caution that the combined effect of rippled structures and non-homogeneous current distributions should be taken seriously for experiments subjected by in-plane magnetic fields.

I. INTRODUCTION

A Josephson junction, formed by two superconducting electrodes connected through a weak link, e.g., a tunnel barrier, a short constriction or a normal metal, can support a non-dissipative Josephson current when the phase difference between the two superconducting electrodes is present. Introducing Zeeman effect into Josephson junctions is not only of fundamental significance in exploring interesting physical phenomena, such as Fulde-Ferrell-Larkin-Ovchinnikov (FFLO) state [1, 2], anomalous Josephson effect [3, 4], planar topological superconductivity [5–8], and Josephson diode effect [9–12], but could have practical applications in superconducting spintronics [13], quantum computing [13, 14], superconducting computing [15, 16], and cryogenic memory [17].

In principle, the Zeeman effect can lead to spin-polarized Fermi surface in which Cooper pairs attaining a finite center-of-mass momentum can survive. The finite Cooper pair momentum manifests itself as a spatially varying term embedded in the superconducting order parameter [18], which can cause the ground state of the Josephson junction to shift by a π phase, known as a π

junction. The π junction has been extensively studied in ferromagnet Josephson junctions [19–24]. Only recently the Zeeman effect-induced π junction has been experimentally reported in systems of semiconductors [25, 26], semimetals [27, 28], and topological insulators [29]. The suppression-and-revival features of the supercurrent was experimentally assigned as the characteristic of Zeeman-driven $0 - \pi$ transition. However, it was recently pointed out that the orbital effect inevitably introduced by rippled structures, which come from the height variations of the non-ideally flat geometry in realistic systems, can give rise to magnetic field components perpendicular to the local surface plane of the sample, and thus lead to supercurrent suppression-and-revival behavior mimicking the true $0 - \pi$ transition [30, 31]. Consequently, when the phase coherent transport concerning in-plane magnetic fields is investigated, extra care must be paid to the effect of ripples.

In this work, we study Josephson junctions with NbTiN weak links using Bi₂O₂Se flakes as a bolster. Naturally, the weak link of NbTiN electrodes is formed at the flake edge due to the height difference between the top of the flake and the Si/SiO₂ substrate. The junctions exhibit supercurrent characteristics similar to usual Josephson junctions, including quantum interference effect in a perpendicular magnetic field and Shapiro steps under a microwave irradiation (Supplemental Material, Sec. IV [32]). Instead of the regular Fraunhofer-like pattern,

* These authors contributed equally to this work.

† lilu@iphy.ac.cn

‡ fanmingqu@iphy.ac.cn

however, the junction displays an interference pattern similar as a superconducting quantum interference device (SQUID), which indicates a non-homogeneous current distribution in the junction [33–39]. Upon application of an in-plane magnetic field, the interference pattern exhibits a unique evolution with each node opened and extended in a V-shape, presenting a diamond-like structure and a false Zeeman-driven $0-\pi$ transition. Theoretically we explore the orbital effect of rippled structures, and find that such a special evolution pattern can be generated in response to a combination of ripples and a certain current distribution. Our results can serve as a caution that the combined effect of rippled structures and non-homogeneous current distributions should be taken seriously when investigating planar Josephson junctions in an in-plane magnetic field.

II. TRANSPORT CHARACTERISTICS

We fabricated NbTiN weak-link junctions through a standard electron-beam lithography technique using $\text{Bi}_2\text{O}_2\text{Se}$ flakes as a bolster. NbTiN film with a thickness of ~ 65 nm was sputtered onto $\text{Bi}_2\text{O}_2\text{Se}$ flakes (~ 30 nm thick). Due to the height difference between the top of the flake and the Si/SiO₂ substrate, the weak link of NbTiN was formed at the flake edge naturally. Devices were then wire-bonded and measured in a cryo-free $^3\text{He}/^4\text{He}$ dilution refrigerator equipped with a three-axis vector magnet and reaching a base temperature of $T = 10$ mK. The transport measurements were carried out in a quasi-four terminal configuration using standard lock-in techniques.

We focus on Josephson junction A (JJA) in the main text, and present the results for JJB in the Supplemental Material, Sec. V [32]. Figure 1(a) shows the measured differential resistance of JJA as a function of current bias I (red curve). The characteristic switching behavior between superconducting and dissipative states is observed at critical supercurrent $I_c \cong 185$ nA. The integrated voltage-current ($V-I$) curve is shown in Fig. 1(a) by the green curve. At high bias the dissipative state corresponds to a resistance $R_N \cong 310$ Ω . Extrapolating the normal-state section of the $V-I$ curve to zero voltage yields an excess current $I_e = 78.3$ nA (as shown by the dot dashed lines). Employing the electron-phonon coupling strength $2\Delta = 3.9 k_B T_c$ and adopting critical temperature $T_c \sim 10$ K for NbTiN electrode, a superconducting gap $\Delta = 1.68$ meV is derived [40]. We can obtain $I_c R_N \sim 57$ μeV and $I_e R_N \sim 24.3$ μeV . These values are significantly smaller than the superconducting gap, indicating a low junction transparency based on the Blonder-Tinkham-Klapwijk (BTK) theory [41, 42].

Next, we present the superconducting interference results when applying a magnetic field B_z perpendicular to the junction plane. Figure 1(b) shows dV/dI as a function of B_z and I . Instead of the regular Fraunhofer-like pattern, a SQUID-like interference pattern is observed,

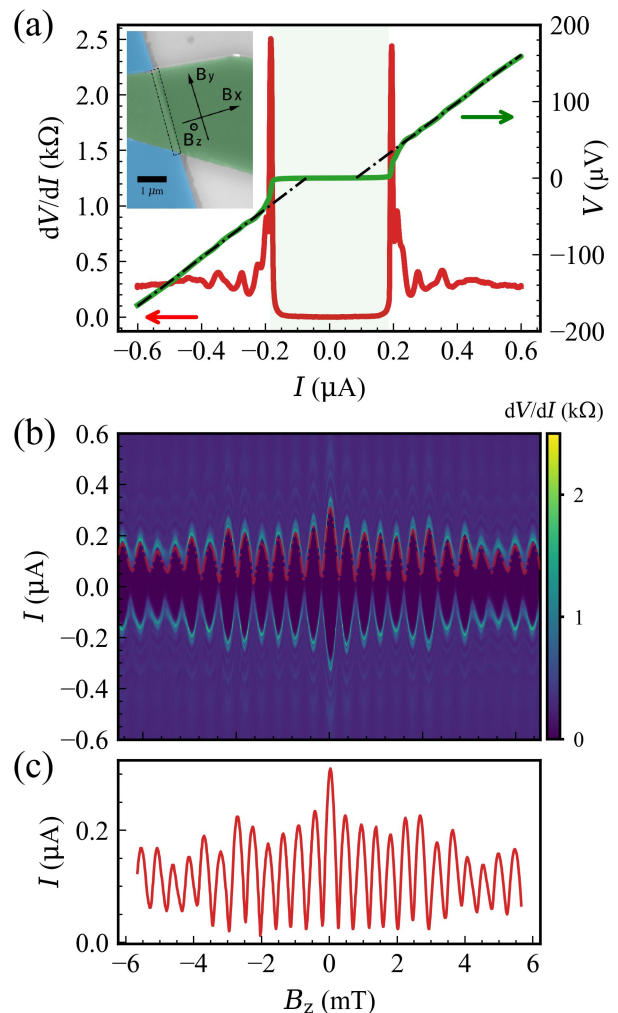


FIG. 1. (a) Differential resistance as a function of current bias (I) at $T = 10$ mK (red), and the integrated voltage-current ($V-I$) curve (green). The black dot-dashed lines are linear fits to the $V-I$ curve at large $|V|$. False-color scanning electron microscope image of Josephson junction A (JJA) is shown in the inset. NbTiN superconducting electrode (green) (~ 65 nm thick) stretches across the edge of the $\text{Bi}_2\text{O}_2\text{Se}$ flake (blue) (~ 30 nm thick) where the weak-link junction forms. (b) Differential resistance as a function of current bias and external perpendicular magnetic field B_z , displaying a SQUID-like interference pattern. The critical supercurrent (I_c) (red curve) is identified by a threshold value (82.3 Ω) below which we attribute to the superconducting state. (c) The extracted critical supercurrent (I_c) [the same as the red curve in (b)].

which indicates a non-homogeneous current distribution in the junction [33–39]. The apparent period is ~ 0.5 mT corresponding to an effective area 4 μm^2 . Based on the expected period $\Phi_0 / [(L_{eff} + 2\lambda_L)W]$ with flux quantum $\Phi_0 = h/2e$, the geometric width of the junction $W \sim 4$ μm , and the London penetration length $\lambda_L = 350$ nm [43, 44], we can get an effective junction length $L_{eff} \sim 300$ nm. Note that L_{eff} could be smaller if considering the flux focusing effect. The SQUID-like inter-

ference pattern appeared in a single Josephson junction is generally regarded as a powerful signature to uncover the edge-dominated supercurrent in previous studies [34–39]. However, a close scrutiny of the extracted critical supercurrent curve, depicted in Fig. 1(c), reveals discrepancies from the regular SQUID interference pattern: the peaks of side lobes far away from the central lobe exhibit an anomalous alternating behavior, rather than a monotonic decreasing behavior in regular SQUIDs. An alternating behavior could arise when an effective three-channel current distribution is involved, as reported in Ref. [34, 45, 46], in which the underlying mechanism could be associated with crossed Andreev reflection. We will interpret our anomalous behavior later.

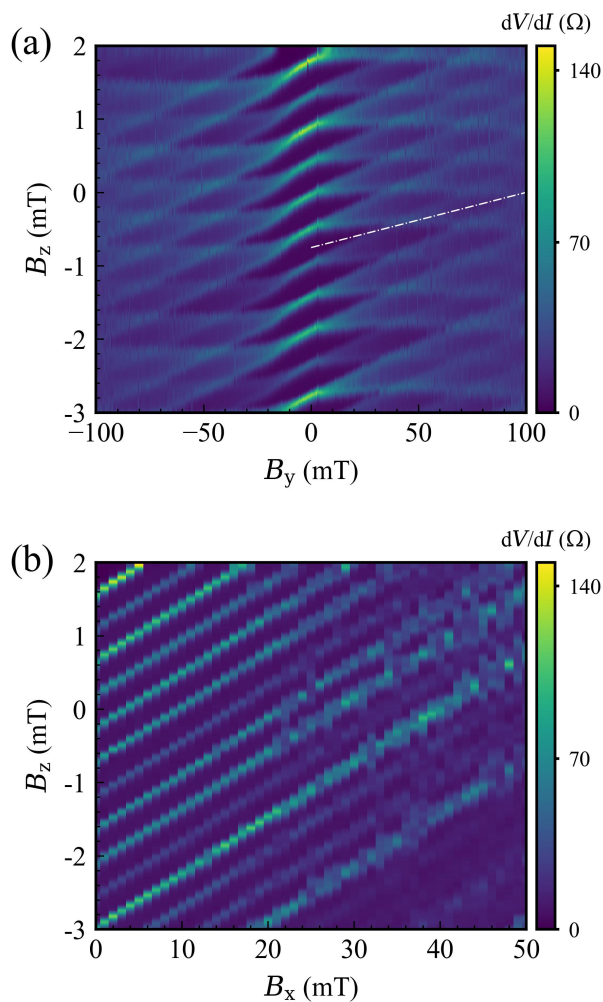


FIG. 2. Evolution of the interference pattern. (a) Interference pattern in an in-plane magnetic field (B_y) perpendicular to the current direction, displaying a V-shaped extension of side nodes imposed on an overall shift. (b) Interference pattern in an in-plane magnetic field (B_x) parallel to the current direction, showing a simple overall shift.

III. TRANSPORT IN IN-PLANE MAGNETIC FIELDS

We next turn our focus to the response of the device to an in-plane magnetic field. To probe the evolution of the interference pattern in an in-plane magnetic field, we apply a small AC excitation (40 nA) and measure the differential resistance dV/dI as a function of B_z and B_y (or B_x), where a lower resistance corresponds to a higher critical supercurrent, and vice versa, similar to that reported in Ref. [25, 29]. When an in-plane magnetic field B_y along the junction width direction (perpendicular to the current) is applied, the evolution of the interference pattern for JJA is shown in Fig. 2(a). As B_y is applied, the interference pattern is shifted along B_z . This is evident as an overall tilt of the 2D differential resistance map in Fig. 2(a), which is caused by the misalignment of the sample with respect to the $B_x - B_y$ plane. A similar shift in the interference pattern caused by such misalignment can also be found when an in-plane magnetic field (B_x) along the current is applied, as shown in Fig. 2(b). Comparatively, we can confirm sample misalignment as the reason for the overall shift of the interference pattern.

Besides the overall shift, we also observe additional side branch features in Fig. 2(a). At $B_y = 0$, the critical supercurrent is minimum at each node (dV/dI peaks). But as B_y is increased, each node splits into two branches and stretches out in a V-shape, presenting a diamond block diagram. Notably, the split branches stretch out and eventually cross each other forming the nodes of the diamonds. Since there is an inverse correlation between dV/dI and the critical supercurrent I_c , if we trace the I_c along the diagonal direction of the diamond pattern as indicated by the white dot-dashed line in Fig. 2(a), we can obtain a suppression-and-recovery behavior, in closer resemblance of suppression-recovery patterns signifying the $0-\pi$ transition reported in ferromagnet Josephson junctions [19–24] and 2D systems [25–27, 29].

In contrast, similar evolution is absent when B_x along the current direction is applied as shown in Fig. 2(b), and only a overall tilt is exhibited.

Some particular types of evolution of the interference pattern in an in-plane magnetic field has recently been predicted theoretically [30] and reported experimentally in rippled graphene Josephson junctions [31], in which the orbital effect induced by the spatial variation of rippled structures is considered to play an important role. In what follows, we give a qualitative discussion of a possible mechanism by focusing on the orbital effect of ripples in line with the framework developed in Ref. [30]. Notably, the Zeeman effect can be safely disregarded owing to the relatively small magnetic field applied in our experiment, compared to the order of several Tesla relevant to the Zeeman-driven $0 - \pi$ transition [26, 27].

IV. THEORETICAL MODEL AND DISCUSSION

To shed light on the origin of the unique diamond-shaped evolution of the interference pattern, we begin by considering the effect of magnetic fields on the phase of the superconducting order parameter. When a magnetic field is threading the junction area, the Aharonov–Bohm effect leads to spatial modulation of gauge invariant phase which manifests itself as a spatially oscillating current according to the Josephson relationship. If a sinusoidal current phase relation is assumed, the Josephson current (I_s) can be determined by the following phase dependent spatial integration,

$$I_s = \int_{-W/2}^{W/2} J_s(y) \sin \left(\varphi - \frac{2e}{\hbar} \int_{-L/2}^{L/2} A(x, y) dx \right) dy \quad (1)$$

where the integral is carried out over the junction width W , φ is the superconductor phase difference, and J_s is the Josephson current density with y the real-space coordinate along the junction width direction. If we assume a uniform current density $J_s(y) = J_0$ and take the unique gauge, $A = -B_z y$ in which the vector potential is parallel to x axis to capture the perpendicular magnetic field B_z , the characteristic Fraunhofer diffraction arises.

$$\begin{aligned} I &= J_0 \int_{-W/2}^{W/2} \sin \left(\varphi + 2\pi \frac{\Phi \cdot y}{\Phi_0 W} \right) dy \\ &= J_0 W \sin(\varphi) \frac{\sin(\pi\Phi/\Phi_0)}{\pi\Phi/\Phi_0} \end{aligned} \quad (2)$$

with $\Phi = B_z L W$ denoting the external magnetic flux enclosed by the junction.

In fact, the presence of an applied in-plane magnetic field can introduce a small component of perpendicular magnetic field due to the not perfectly flat surface accompanied by spatial height variations. Hence, the vector potential modulation comes into play. As pointed out in Ref. [30], the rippled structure can give rise to an orbital effect which can lead to critical supercurrent oscillation in parallel magnetic fields. For simplicity, rippled structure with height distributions η can be depicted by the cosines functions,

$$\eta(x, y) = \frac{\eta_0}{2} \cos \left(n\pi \frac{x}{L} \right) \cos \left(m\pi \frac{y}{W} \right) \quad (3)$$

where η_0 is the peak-to-peak height difference. Eq. (3) captures n uniform ripples in the x direction (junction length direction) and m uniform ripples in the y direction (junction width direction). The orbital effect induced by ripples manifests itself as a modulation of vector potential as follows,

$$\int_{L/2}^{L/2} A(x, y) dx = B_y L \bar{\eta}(y) - B_z L y \quad (4)$$

where $\bar{\eta}$ is the longitudinally averaged height.

$$\bar{\eta}(y) = \frac{1}{L} \int_{-L/2}^{L/2} \eta(x, y) dx \quad (5)$$

Based on Eq. (3), the ripples can be categorized into short- and long-wavelength ones. The short-wavelength one appears as rapidly oscillating terms averaging to a small value in the integral of Eq. (5), and thus contributes little to the modulation. Nevertheless, the cumulative effect of short ripples can cause a faster decay of the critical supercurrent due to large orbital depairing effect as elaborated in Ref. [30]. Intuitively, the effect of a ripple can be gauged by enclosed flux within the effective ripple area. In order to induce a zero crossing of the critical supercurrent, the in-plane magnetic field needs to reach $B_0 = \Phi_0/4L\eta_0$ [30]. In our experimental configuration of JJA, with an effective junction length $L_{eff} \sim 300$ nm and η_0 approximated by the vertical height difference of roughly 30 nm, we evaluate $B_0 \sim 55$ mT, slightly larger than the experimental value ~ 40 mT. This discrepancy could be accounted by the contributions of short ripples unidentified in the realistic system, which cause a sharper decay of the critical supercurrent [30], or the uncertainty of L_{eff} .

To gain more insight into the observed diamond block diagram, the evolution of the interference pattern can be

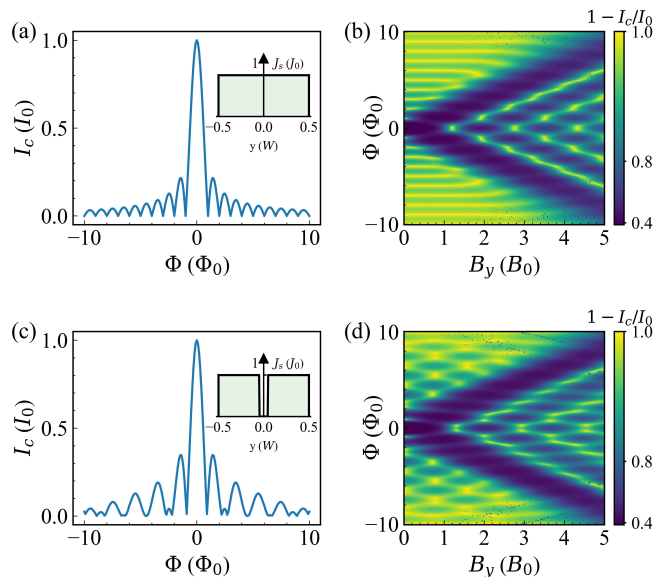


FIG. 3. Calculated interference patterns in an in-plane magnetic field B_y under specific current distribution conditions. (a) Homogeneous current distribution (inset) displays standard Fraunhofer pattern at zero in-plane magnetic field. (b) The evolution of the interference pattern in B_y for the homogeneous current distribution shown in (a), where bright yellow color denotes zero critical supercurrent (dark blue corresponds to large critical supercurrent). (c) and (d) The case of a concave shaped current distribution. Here B_0 corresponds to the in-plane magnetic field that could suppress the critical supercurrent to zero, $B_0 = \Phi_0/4L\eta_0$.

attained using the phenomenological model given above [Eq. (1)]. To begin with, we consider a long-wavelength ripple structure with a height distribution depicted by Eq. (5) with $n=1$ and $m=2$, along with a uniform Josephson current density. We can obtain the evolution of the Fraunhofer pattern in an in-plane magnetic field incorporating the orbital effect induced by the rippled structures, as shown in Figs. 3 (a,b), consistent with Ref. [30]. Subsequently, we allow for the deviation from the uniform current distribution and consider a non-homogeneous current distribution with a two-channel step-like shape, as illustrated in the inset in Fig. 3 (c). The evolution of the interference pattern develops a unique evolutionary characteristic in which each side node is opened and stretched out in a V-shape as displayed in Fig. 3 (d), similar to the experimental results. Such evolution results from the interference between the two-channel vector potential phase in response to the orbital effect of the rippled structure.

However, for our results on JJA, the superconducting interference pattern at zero in-plane magnetic field displays a SQUID-like interference pattern but with sig-

nificant discrepancies, as shown in Figs. 1 (b, c). As explained above, the alternating behavior of the critical supercurrent indicates a three-channel current distribution, as reported in [34, 45, 46]. Based on this, we further postulate a special three-channel step-like current distribution, as sketched in the inset of Fig. 4 (a), and demonstrate that a better qualitative agreement could be achieved between the modeled evolution of the interference pattern and the observed diamond block diagram. The corresponding interference pattern in an in-plane field is shown in Fig. 4 (b), involving the same rippled structure as Fig. 3 with $n=1$ and $m=2$. The main feature that each node opened and stretched out is developed. When we further reduce the width of the current channels, as revealed in Figs. 4 (c-f), a better qualitative agreement with the experimental results shown in Fig. 2(a) is achieved. The oscillating critical supercurrent and the main features of the diamond block diagram are reconstructed, with each side node opened and stretched out in a V-shape, as displayed in Figs. 4 (e) and (f). It should be mentioned that although it is enigmatic to exhibit three current channels, we speculate that it is possible to present equivalently three channels in the junction since the not well-defined junction region is naturally formed at the flake edge and the qualitative agreement has been realized between the model and the experimental results. Such geometry with lateral height difference makes it physically conceivable due to the extreme strain and curvature at the edges where the junction sustains. Noteworthy, despite the rippled effect in combination with specific current distributions, we yet cannot exclude the possibility in which other mechanisms can come into play.

V. CONCLUSION

In conclusion, a unique evolution of the superconducting interference pattern is observed in NbTiN weak-link Josephson junctions subjected in an in-plane magnetic field. The evolution pattern manifests itself as a diamond block diagram featured with each side node opened and stretched out in a V-shape, mimicking the suppression-recovery patterns of critical supercurrent related to Zeeman-driven $0 - \pi$ transition. In our case, we securely rule out the influence of Zeeman effect as the involved magnetic field is as small as dozens of millitesla and restrict our attention to the trivial orbital effect induced by rippled structures. The lateral height difference of the junction makes it easier to accumulate a flux quantum within a long-wavelength ripple, and meanwhile suppresses the critical supercurrent rapidly, which can induce a suppression-recovery behavior in a relatively small magnetic field.

Through a phenomenological formulation of rippled structures, we expand the phase modulation analysis developed in Ref. [30], by introducing several specific non-uniform current distributions. We find that a certain

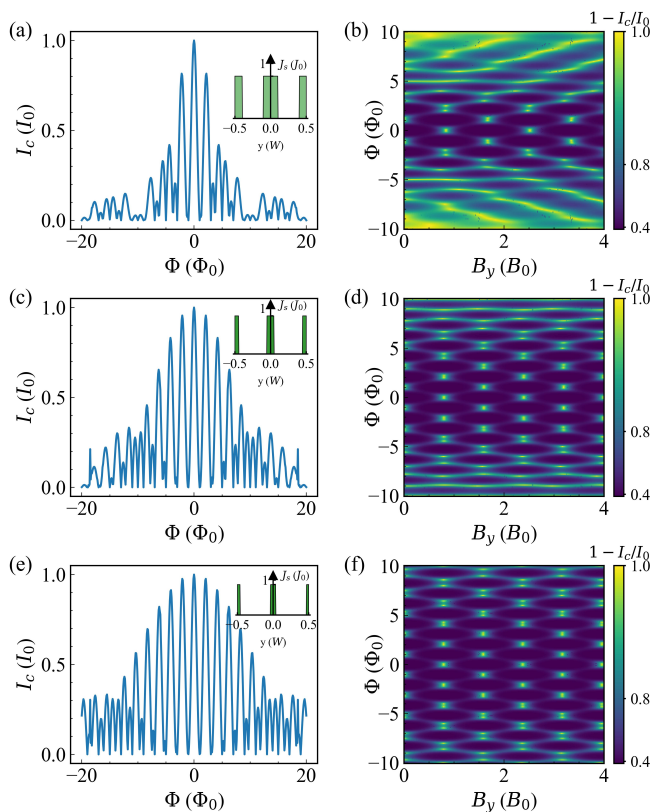


FIG. 4. Calculated interference patterns in an in-plane magnetic field B_y under a three-channel current distribution. (a) The interference pattern for the specific current distribution sketched in the inset at zero in-plane magnetic field. (b) The evolution of the interference pattern in B_y for the current distribution shown in (a). (c, d) and (e, f) The same as (a, b), but for a decreased width of the current channels.

current distribution gives rise to a specific corresponding evolution of the superconducting interference pattern in an in-plane magnetic field. By considering two- and three-channel step-like current distributions, similar diamond block diagrams as the observations can be reproduced. A qualitative agreement is achieved for a three-channel distribution and a given rippled structure.

Our results serve as a caution that the combined effect of rippled structures and non-homogeneous current distributions should be taken seriously when the phase coherent transport involving in-plane magnetic fields is explored. Further effort is required to uncover the complex effect of these ingredients, and the induced trivial misguide behaviors demand more attention when investigating phenomena concerning superconducting and topological properties.

ACKNOWLEDGMENTS

This work was supported by the National Key Research and Development Program of China (2022YFA1403400 and 2017YFA0304700), by the NSF China (12074417, 92065203, and 11774405), by the Strategic Priority Research Program B of Chinese Academy of Sciences (XDB28000000 and XDB33000000), by the Synergetic Extreme Condition User Facility sponsored by the National Development and Reform Commission, and by the Innovation Program for Quantum Science and Technology (2021ZD0302600).

-
- [1] P. Fulde and R. A. Ferrell, *Phys. Rev.* **135**, A550 (1964).
 [2] Y. N. O. A.I. Larkin, *J. Exp. Theor. Phys.* **28**, 1200 (1964).
 [3] T. Yokoyama, M. Eto, and Y. V. Nazarov, *Phys. Rev. B* **89**, 195407 (2014).
 [4] D. B. Szombati, S. Nadj-Perge, D. Car, S. R. Plissard, E. P. A. M. Bakkers, and L. P. Kouwenhoven, *Nat. Phys.* **12**, 568 (2016).
 [5] M. Hell, M. Leijnse, and K. Flensberg, *Phys. Rev. Lett.* **118**, 107701 (2017).
 [6] F. Pientka, A. Keselman, E. Berg, A. Yacoby, A. Stern, and B. I. Halperin, *Phys. Rev. X* **7**, 021032 (2017).
 [7] A. Fornieri, A. Whiticar, F. Setiawan, *et al.*, *Nature* **569**, 89 (2019).
 [8] H. Ren, F. Pientka, S. Hart, *et al.*, *Nature* **569**, 93 (2019).
 [9] M. Davydova, S. Prembabu, and L. Fu, *Sci. Adv.* **8**, eabo0309 (2022).
 [10] B. Pal, A. Chakraborty, P. K. Sivakumar, M. Davydova, *et al.*, *Nat. Phys.* **18**, 1228 (2022).
 [11] F. Ando, Y. Miyasaka, T. Li, J. Ishizuka, T. Arakawa, Y. Shiota, T. Moriyama, Y. Yanase, and T. Ono, *Nature* **584**, 373 (2020).
 [12] H. Wu, Y. Wang, Y. Xu, P. K. Sivakumar, C. Pasco, *et al.*, *Nature* **604**, 653 (2022).
 [13] J. Linder and J. W. A. Robinson, *Nat. Phys.* **11**, 307 (2015).
 [14] G. Blatter, V. B. Geshkenbein, and L. B. Ioffe, *Phys. Rev. B* **63**, 174511 (2001).
 [15] A. Feofanov, V. Oboznov, V. Bol'ginov, *et al.*, *Nat. Phys.* **6**, 593 (2010).
 [16] A. V. Ustinov and V. K. Kaplunenko, *J. Appl. Phys.* **94**, 5405 (2003).
 [17] E. Gingrich, B. Niedzielski, J. Glick, *et al.*, *Nat. Phys.* **12**, 564 (2016).
 [18] A. I. Buzdin, *Rev. Mod. Phys.* **77**, 935 (2005).
 [19] T. Kontos, M. Aprili, J. Lesueur, F. Genêt, B. Stephanidis, and R. Boursier, *Phys. Rev. Lett.* **89**, 137007 (2002).
 [20] W. Guichard, M. Aprili, O. Bourgeois, T. Kontos, J. Lesueur, and P. Gandit, *Phys. Rev. Lett.* **90**, 167001 (2003).
 [21] Y. Blum, A. Tsukernik, M. Karpovski, and A. Palevski, *Phys. Rev. Lett.* **89**, 187004 (2002).
 [22] V. A. Oboznov, V. V. Bol'ginov, A. K. Feofanov, V. V. Ryazanov, and A. I. Buzdin, *Phys. Rev. Lett.* **96**, 197003 (2006).
 [23] V. Shelukhin, A. Tsukernik, M. Karpovski, Y. Blum, K. B. Efetov, A. F. Volkov, T. Champel, M. Eschrig, T. Löfwander, G. Schön, and A. Palevski, *Phys. Rev. B* **73**, 174506 (2006).
 [24] J. W. A. Robinson, S. Piano, G. Burnell, C. Bell, and M. G. Blamire, *Phys. Rev. Lett.* **97**, 177003 (2006).
 [25] S. Hart, H. Ren, M. Kosowsky, G. Ben-Shach, P. Leubner, C. Brüne, H. Buhmann, L. W. Molenkamp, B. I. Halperin, and A. Yacoby, *Nat. Phys.* **13**, 87 (2016).
 [26] C. T. Ke, C. M. Moehle, F. K. de Vries, C. Thomas, S. Metti, C. R. Guinn, R. Kallagher, M. Lodari, G. Scappucci, T. Wang, R. E. Diaz, G. C. Gardner, M. J. Manfra, and S. Goswami, *Nat. Commun.* **10**, 3764 (2019).
 [27] C. Li, B. de Ronde, J. de Boer, J. Ridderbos, F. Zwanenburg, Y. Huang, A. Golubov, and A. Brinkman, *Phys. Rev. Lett.* **123**, 026802 (2019).
 [28] C. Li, J. C. de Boer, B. de Ronde, S. V. Ramankutty, *et al.*, *Nat. Mater.* **17**, 875 (2018).
 [29] A. Q. Chen, M. J. Park, S. T. Gill, Y. Xiao, I. P. D. Reig, G. J. MacDougall, M. J. Gilbert, and N. Mason, *Nat. Commun.* **9**, 3478 (2018).
 [30] E. H. Fyhn, M. Amundsen, A. Zalic, T. Dvir, H. Steinberg, and J. Linder, *Phys. Rev. B* **102**, 024510 (2020).
 [31] T. Dvir, A. Zalic, E. H. Fyhn, M. Amundsen, T. Taniguchi, K. Watanabe, J. Linder, and H. Steinberg, *Phys. Rev. B* **103**, 115401 (2021).
 [32] See Supplemental Material.
 [33] M. Popinciuc, V. E. Calado, X. L. Liu, A. R. Akhmerov, T. M. Klapwijk, and L. M. K. Vandersypen, *Phys. Rev. B* **85**, 205404 (2012).
 [34] V. S. Pribiag, A. J. A. Beukman, F. Qu, M. C. Cassidy, C. Charpentier, W. Wegscheider, and L. P. Kouwenhoven, *Nat. Nanotechnol.* **10**, 593 (2015).
 [35] S. Hart, H. Ren, T. Wagner, P. Leubner, M. Mühlbauer, C. Brune, H. Buhmann, L. Molenkamp, and A. Yacoby, *Nat. Phys.* **10**, 638 (2014).
 [36] D. Sticlet, P. Wójcik, and M. P. Nowak, *Phys. Rev. B* **102**, 165407 (2020).
 [37] J. Ying, J. He, G. Yang, M. Liu, Z. Lyu, X. Zhang, H. Liu,

- K. Zhao, R. Jiang, Z. Ji, J. Fan, C. Yang, X. Jing, G. Liu, X. Cao, X. Wang, L. Lu, and F. Qu, *Nano Lett.* **20**, 2569 (2020).
- [38] M. T. Allen, O. Shtanko, I. C. Fulga, A. R. Akhmerov, K. Watanabe, T. Taniguchi, P. Jarillo-Herrero, L. S. Levitov, and A. Yacoby, *Nat. Phys.* **12**, 128 (2015).
- [39] C. Huang, A. Narayan, E. Zhang, X. Xie, L. Ai, S. Liu, C. Yi, Y. Shi, S. Sanvito, and F. Xiu, *Natl. Sci. Rev.* **7**, 1468 (2020).
- [40] J. Zhi, N. Kang, F. Su, D. Fan, S. Li, D. Pan, S. P. Zhao, J. Zhao, and H. Q. Xu, *Phys. Rev. B* **99**, 245302 (2019).
- [41] K. Flensberg, J. B. Hansen, and M. Octavio, *Phys. Rev. B* **38**, 8707 (1988).
- [42] M. Octavio, M. Tinkham, G. E. Blonder, and T. M. Klapwijk, *Phys. Rev. B* **27**, 6739 (1983).
- [43] L. R. St. Marie, C.-I. Liu, I.-F. Hu, H. M. Hill, *et al.*, *Phys. Rev. B* **104**, 085435 (2021).
- [44] E. F. Talantsev, W. P. Crump, J. O. Island, Y. Xing, Y. Sun, J. Wang, and J. L. Tallon, *2D Mater.* **4**, 025072 (2017).
- [45] F. K. de Vries, T. Timmerman, V. P. Ostroukh, J. van Veen, A. J. A. Beukman, F. Qu, M. Wimmer, B.-M. Nguyen, A. A. Kiselev, W. Yi, M. Sokolich, M. J. Manfra, C. M. Marcus, and L. P. Kouwenhoven, *Phys. Rev. Lett.* **120**, 047702 (2018).
- [46] F. K. de Vries, M. L. Sol, S. Gazibegovic, R. L. M. o. h. Veld, S. C. Balk, D. Car, E. P. A. M. Bakkers, L. P. Kouwenhoven, and J. Shen, *Phys. Rev. Res.* **1**, 032031(R) (2019).
- [47] T. Yamashita, K. Tanikawa, S. Takahashi, and S. Maekawa, *Phys. Rev. Lett.* **95**, 097001 (2005).

Supplemental Material for: "Diamond-shaped evolution of the superconducting interference pattern in NbTiN weak-link Josephson junctions"

Kui Zhao,^{1,2,*} Huaiyuan Liu,^{1,2,*} Jianfei Xiao,^{1,2,*} Linfeng Tu,^{1,3} Jiangbo He,¹ Mingli Liu,^{1,2} Ruiyang Jiang,^{1,2} Zhongmou Jia,^{1,2} Shang Zhu,^{1,2} Yunteng Shi,^{1,2} Yiwen Ma,^{1,2} Zhaozheng Lyu,¹ Jie Shen,^{1,4} Guangtong Liu,^{1,4} Li Lu,^{1,2,4,†} and Fanming Qu^{1,2,4,‡}

¹Beijing National Laboratory for Condensed Matter Physics,
Institute of Physics, Chinese Academy of Sciences, Beijing 100190, China.

²School of Physical Sciences, University of Chinese Academy of Sciences, Beijing 100049, China.

³School of Physics, Nankai University, Tianjin 300071, China.

⁴Songshan Lake Materials Laboratory, Dongguan, Guangdong 523808, China.

(Dated: March 13, 2023)

I. Evolution of the interference pattern under several specific current distributions

In addition to the ones shown in the main text, we further consider several specific current distributions and investigate the corresponding evolution of the interference pattern, as shown in Figs. S1-5. A specific current distribution presents a unique evolution correspondingly. Roughly speaking, the evolution behavior can serve as a fingerprint for the specific current distribution when considering the orbital effect of ripples.

Since the Josephson current density is non-uniform, here we consider the generalized supercurrent density J_s (J_0) along the y axis, as schematically shown in Fig. S1, to capture the step-like nonuniform supercurrent density distributions. S_e (S_c) is the width of the edge-step (center-step) in units of junction width W . The corresponding supercurrent density is normalized by J_0 denoted by J_e (J_c). The rest normalized bulk supercurrent density is denoted by J_b . We can use a set of coordinates $\{S_e : J_e, S_c : J_c, J_b\}$ to describe specified distribution. The parameters used in the main text are, $\{S_e : J_e, S_c : J_c, J_b\} = \{0 : 0, 0 : 0, 1\}$, $\{0.45 : 1, 0 : 0, 0\}$, $\{0.1 : 1, 0.2 : 1, 0\}$, $\{0.05 : 1, 0.1 : 1, 0\}$, $\{0.035 : 1, 0.070 : 1, 0\}$ for Figs. 3(a), 3(c), 4(a), 4(c), 4(e), respectively.

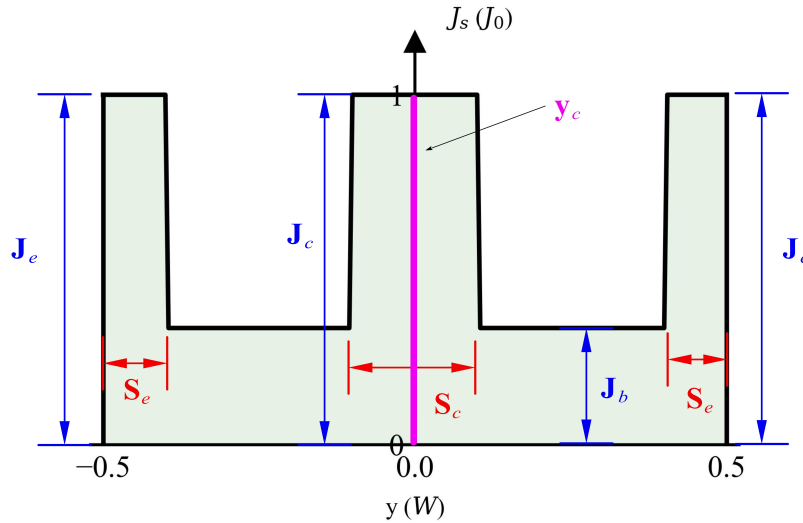


FIG. S1. A schematic of the supercurrent density distribution J_s along the y axis, $\{S_e : J_e, S_c : J_c, J_b\} = \{0.1 : 1, 0.2 : 1, 1/3\}$ for this case.

* These authors contributed equally to this work.

† lilu@iphy.ac.cn

‡ fanmingqu@iphy.ac.cn

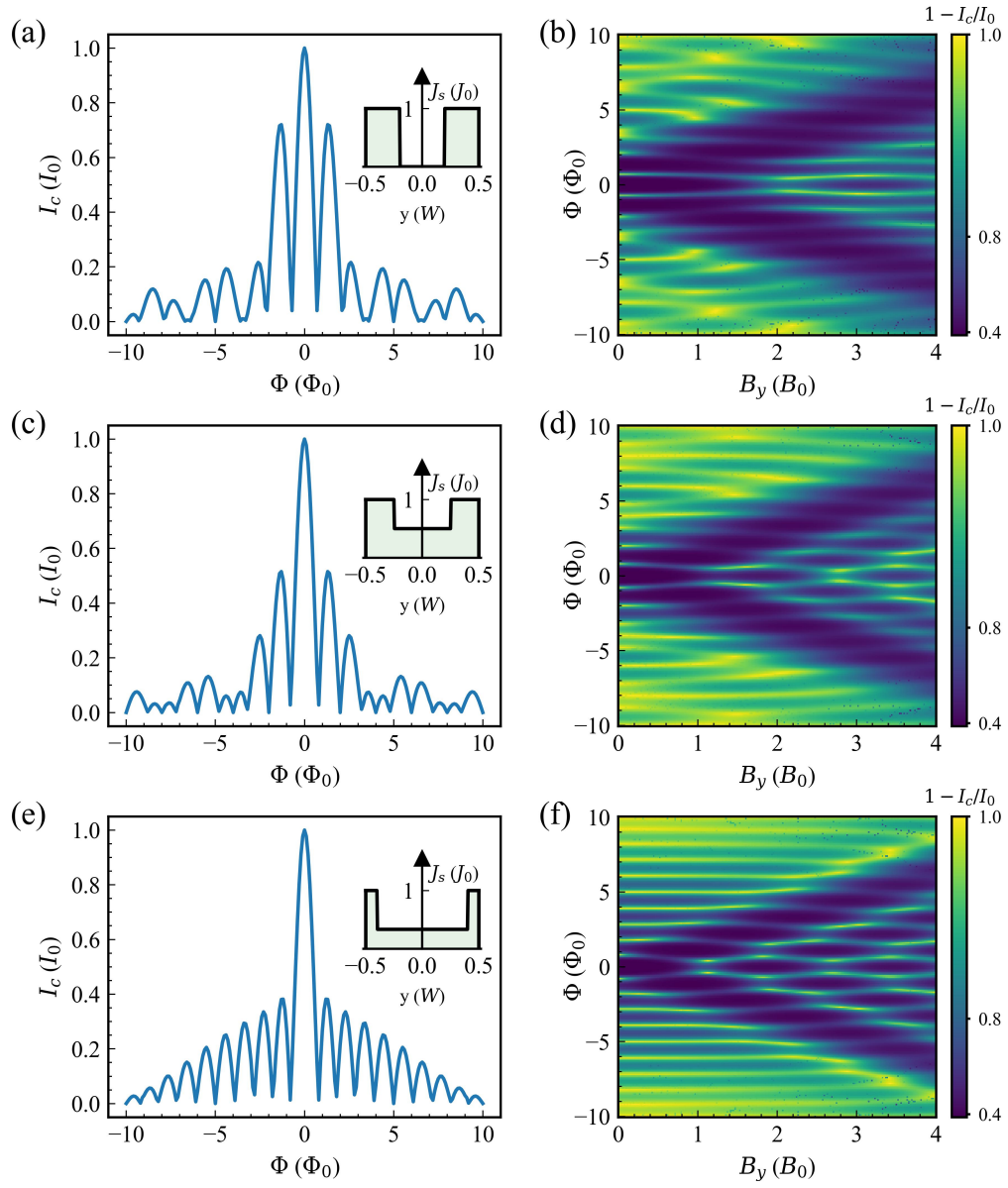


FIG. S2. Calculated interference patterns in an in-plane magnetic field B_y under specific current distribution conditions. $\{S_e : J_e, S_c : J_c, J_b\} = \{0.30 : 1, 0 : 0, 0\}, \{0.25 : 1, 0 : 0, 0.5\}, \{0.10 : 1, 0 : 0, 1/3\}$, for (a, b), (c, d), (e, f), respectively.

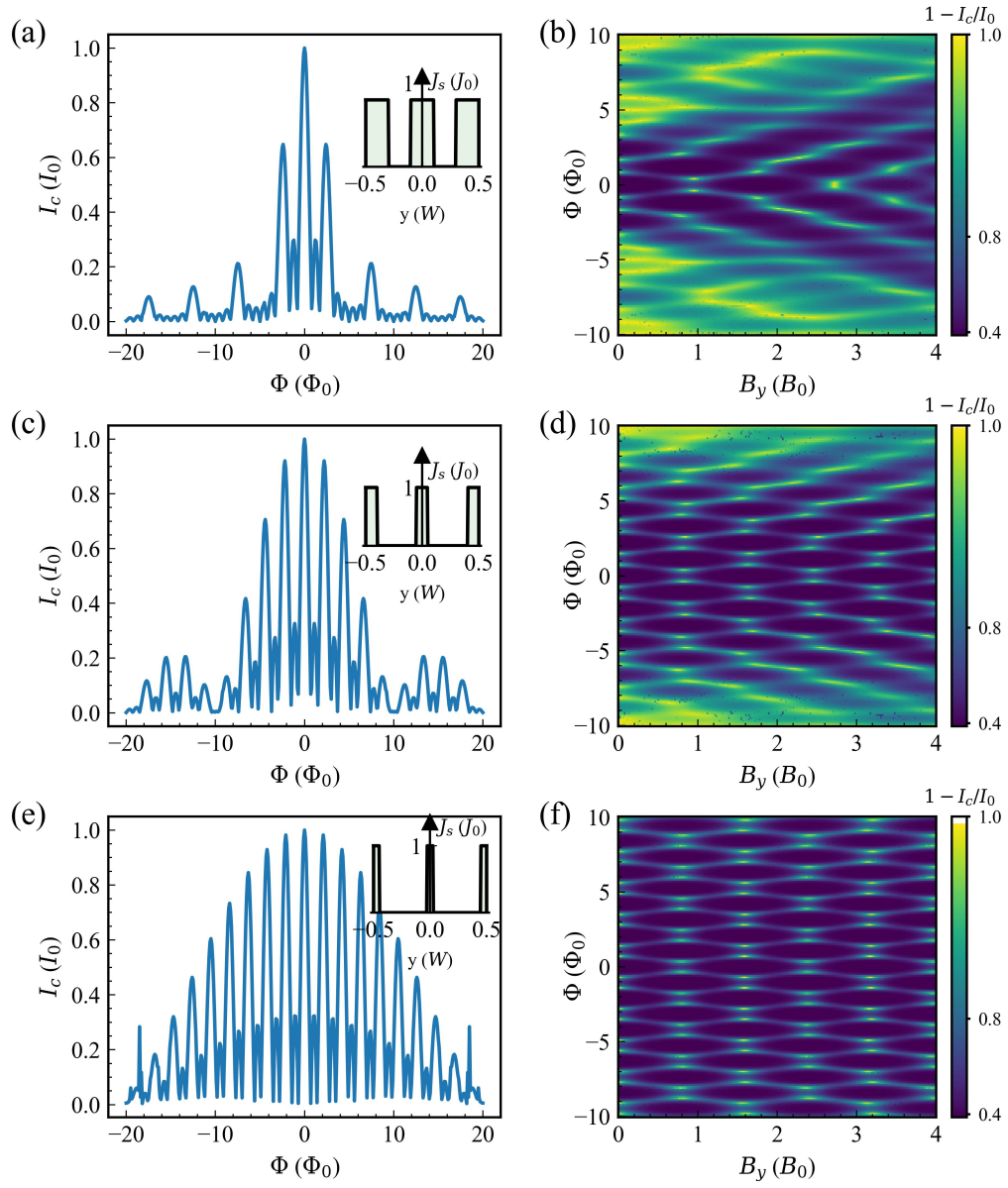


FIG. S3. Calculated interference patterns in an in-plane magnetic field B_y under specific current distribution conditions. $\{S_e : J_e, S_c : J_c, J_b\} = \{0.2 : 1, 0.2 : 1, 0\}, \{0.1 : 1, 0.1 : 1, 0\}, \{0.05 : 1, 0.05 : 1, 0\}$, for (a, b), (c, d), (e, f), respectively.

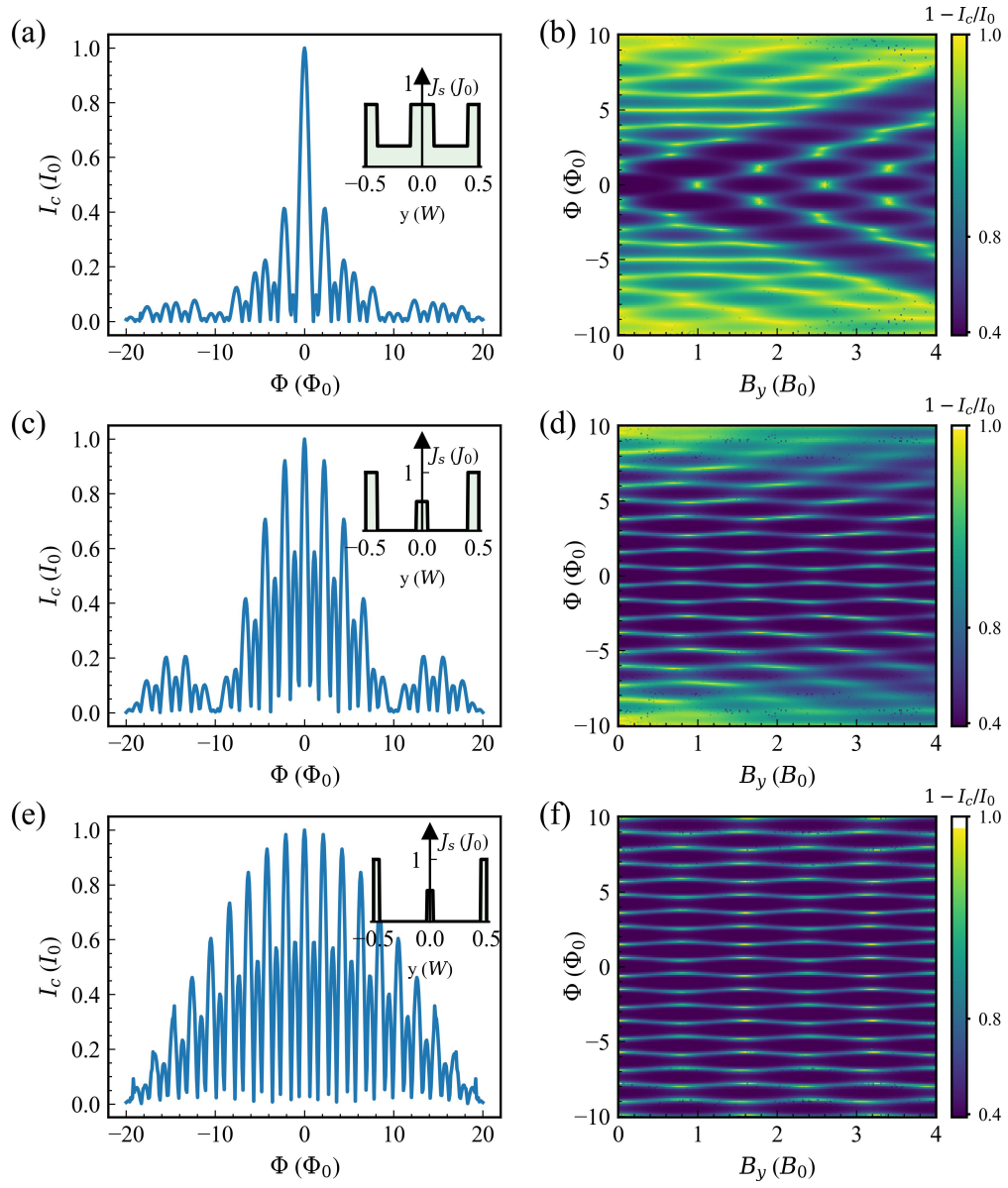


FIG. S4. Calculated interference patterns in an in-plane magnetic field B_y under specific current distribution conditions. $\{S_e : J_e, S_c : J_c, J_b\} = \{0.1 : 1, 0.2 : 1, 1/3\}$, $\{0.1 : 1, 0.1 : 0.5, 0\}$, $\{0.05 : 1, 0.05 : 0.5, 0\}$, for (a, b), (c, d), (e, f), respectively.

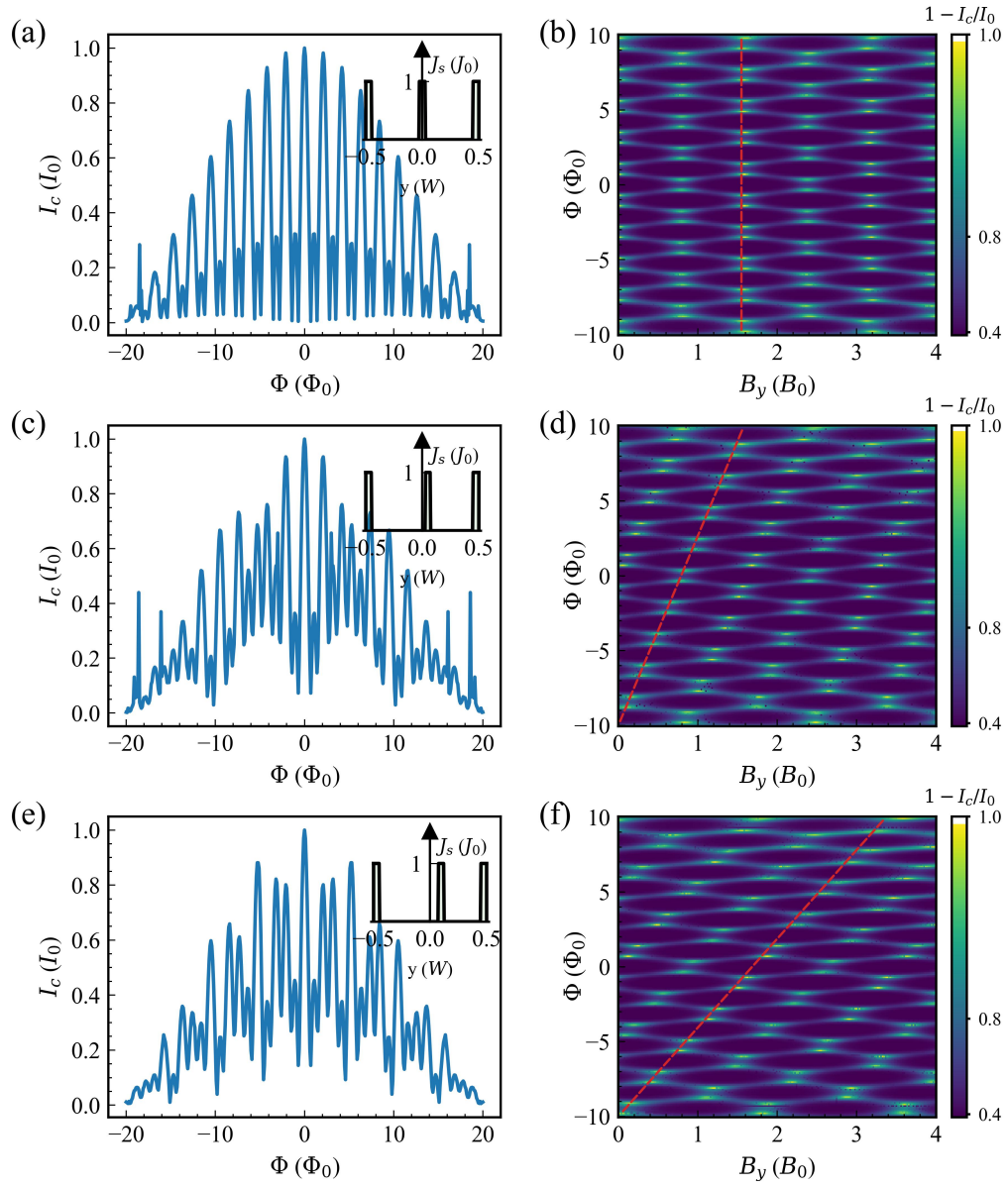


FIG. S5. Calculated interference patterns in an in-plane magnetic field B_y under specific current distribution conditions. $\{S_e : J_e, S_c : J_c, J_b\} = \{0.05 : 1, 0.05 : 1, 0\}$, $y_c = \{0, 0.05, 0.10\}$, for (a, b), (c, d), (e, f), respectively. The red dash line shows a guideline for the overall tilting of the evolution pattern as the position of the central current step deviates from the center of the junction.

II. Temperature dependence of critical supercurrent

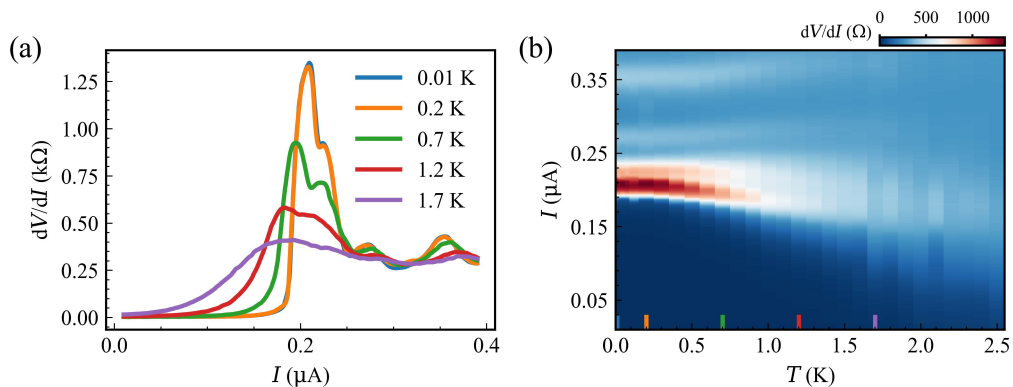


FIG. S6. Temperature dependence of critical supercurrent of JJA. (a) Line-cuts of dV/dI versus I at different temperatures, as indicated by the colored ticks in (b). (b) Color maps of dV/dI versus I and temperature T .

III. Superconducting interference spectra at different in-plane magnetic field B_y

Superconducting interference spectra at specific in-plane magnetic fields B_y is shown in Fig. S7. As can be seen, the interference spectra experiences a special evolution. A suppression-and-revival tendency of the critical supercurrent can be recognized.

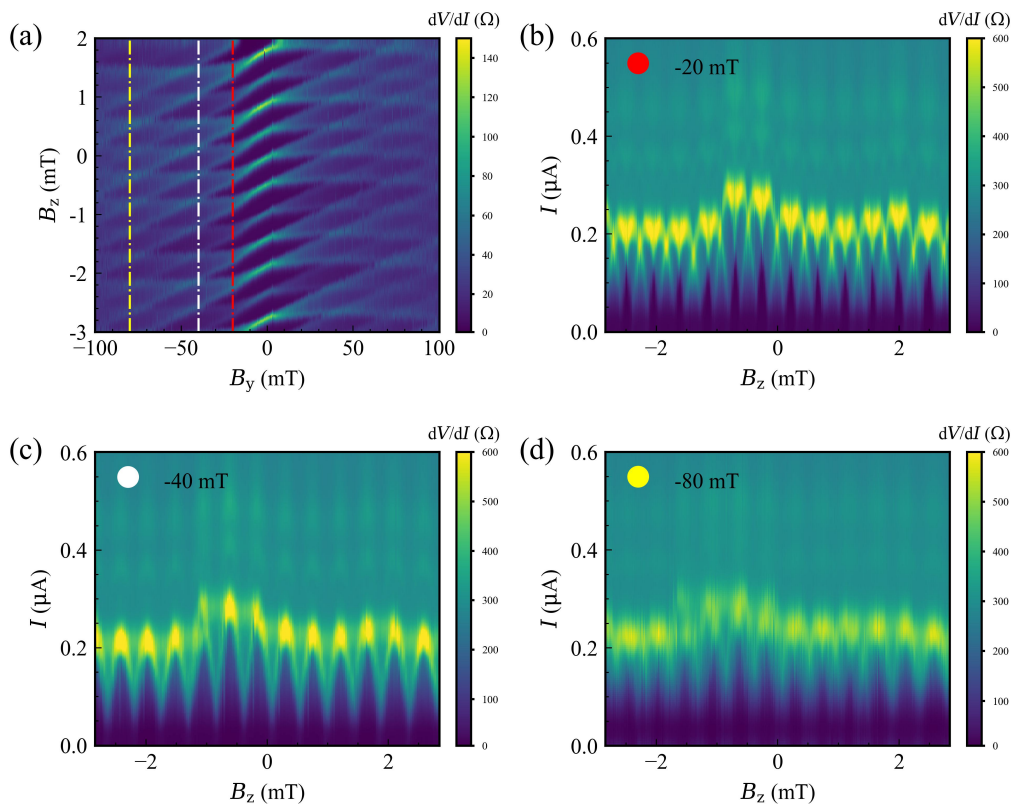


FIG. S7. Superconducting interference spectra at different in-plane magnetic fields B_y . (a) Evolution of the interference pattern in an in-plane magnetic field B_y , the same as Fig. 2(a) in the main text. (b-d) Interference pattern — differential resistance dV/dI as a function of perpendicular magnetic field B_z and bias current I , at $B_y = -20, -40, -80$ mT, respectively, as indicated by the dot-dashed lines in (a).

IV. Shapiro steps under radio-frequency (RF) irradiation

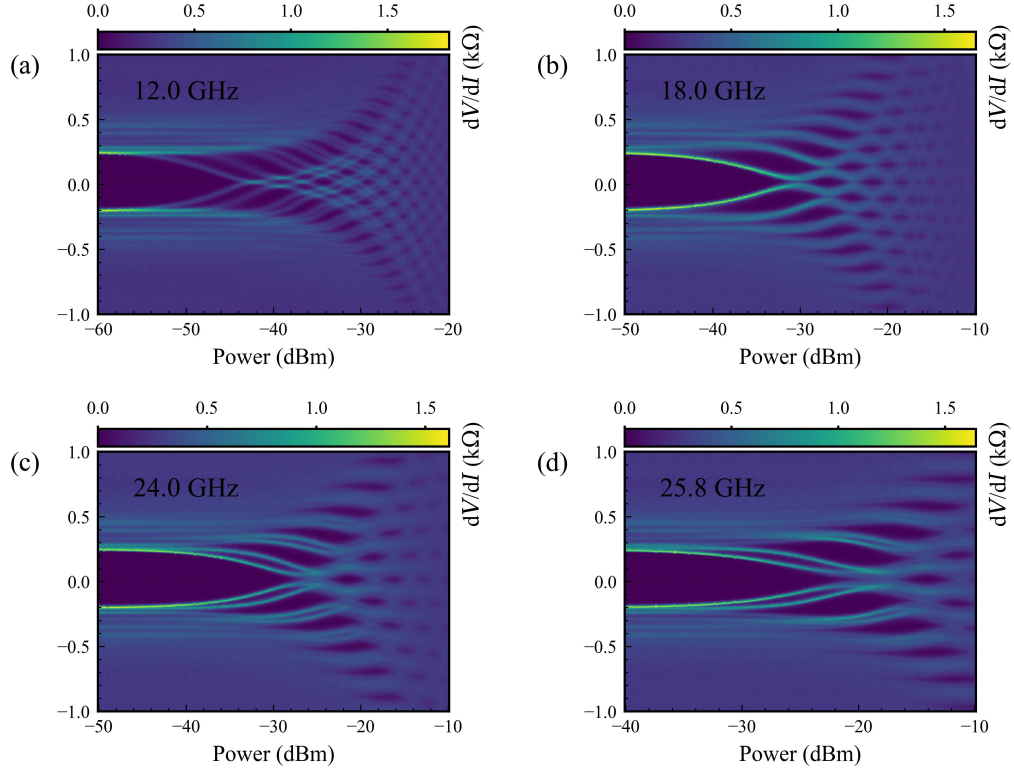


FIG. S8. Radio frequency response of JJA. (a-d) Differential resistance as a function of bias current and RF excitation power at frequencies $f = 12, 18, 24$ and 25.8 GHz, respectively.

We observed the appearance of Shapiro steps in JJA under the radio-frequency (RF) irradiation [Fig. S8]. A RF excitation via an open ended coaxial line was irradiated on the sample. The evolution of the differential resistance as a function of RF excitation power at different RF frequencies is shown in Fig. S8(a-d).

V. Similar interference pattern observed in JJB

A similar evolution of the interference pattern was also observed in JJB, as shown in Fig. S9. Upon application of an in-plane field, the critical supercurrent undergoes a suppression and a transition from a Fraunhofer-like pattern to a superconducting quantum interference device (SQUID)-like pattern [Fig. S9(c)].

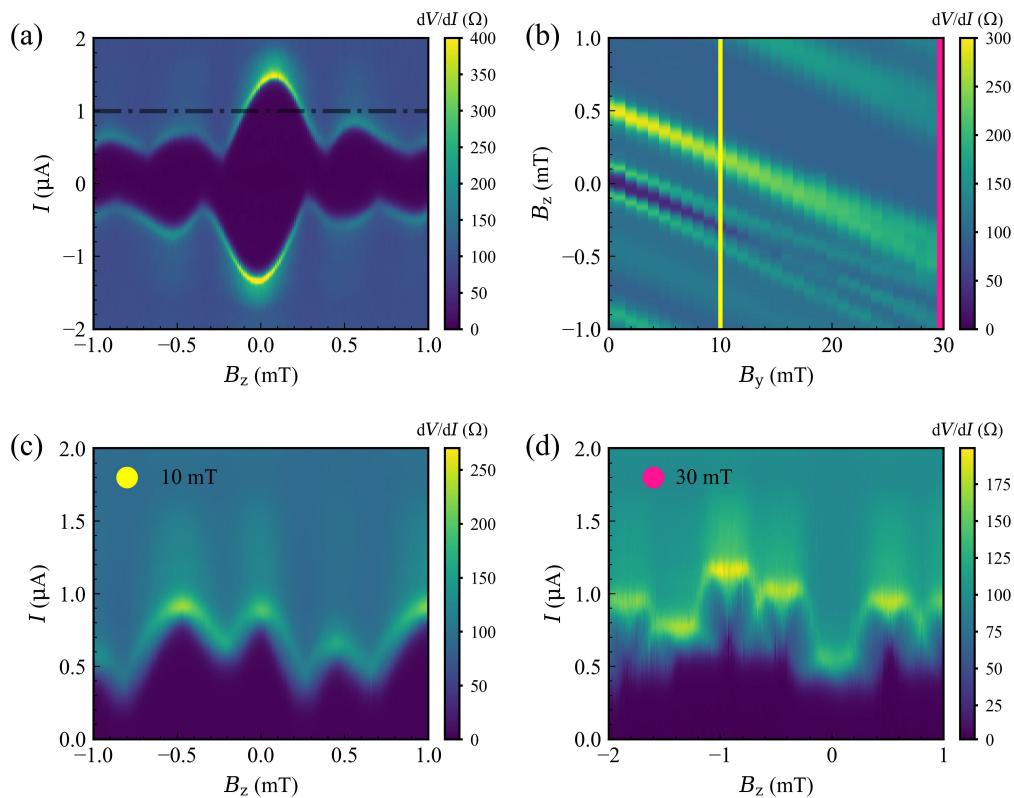


FIG. S9. Evolution of the interference pattern of JJB. (a) Differential resistance map versus I and B_z , exhibits a Fraunhofer-like pattern, revealing a relatively uniform current distribution in JJB. (b) Evolution of the interference pattern versus in-plane magnetic field B_y . Note that the map is obtained with a finite bias current ($I = 1 \mu\text{A}$) as indicated by the black dot-dashed line in (a), differing from $I = 0$ in the case of JJA. (c) and (d) Interference spectra under $B_y = 10, 30$ mT, respectively, corresponding to the solid lines indicated in (b).

The analogous phenomenon is also found in planar graphene Josephson junctions [1], in which the orbital effect of rippled structures is considered to play an important role. In our study, the contributions of the possible Zeeman splitting effect can be safely disregarded due to the small amplitude of the in-plane magnetic field. Therefore, we attribute our observations to the orbital effect of the inevitably existing rippled structures.

[1] T. Dvir, A. Zalic, E. H. Fyhn, M. Amundsen, T. Taniguchi, K. Watanabe, J. Linder, and H. Steinberg, Planar graphene-nbse₂ josephson junctions in a parallel magnetic field, *Phys. Rev. B* **103**, 115401 (2021).